A selfconsistent formulation for the prediction of the anisotropic behavior of viscoplastic polycrystals with voids

R.A. Lebensohn, C.N. Tomé*, P.J. Maudlin

Los Alamos National Laboratory, Los Alamos, NM 87545, USA

Abstract

In this work we consider the presence of ellipsoidal voids inside polycrystals subjected to large strain deformation. For this purpose, the originally incompressible viscoplastic selfconsistent (VPSC) formulation of Lebensohn and Tomé (Acta Metall. Mater. 41 (1993) 2611) has been extended to deal with compressible polycrystals. In doing this, both the deviatoric and the spherical components of strain-rate and stress are accounted for. Such an extended model allows us to account for the void and for porosity evolution, while preserving the anisotropy and crystallographic capabilities of the VPSC model. The formulation can be adjusted to match the Gurson model, in the limit of rate-independent isotropic media and spherical voids. We present several applications of this extended VPSC model, which address the coupling between texture, plastic anisotropy, void shape, triaxiality, and porosity evolution.
© 2003 Elsevier Ltd. All rights reserved.

Keywords: Self-consistent; Polycrystal model; Damage evolution; Voids; Plasticity

1. Introduction

The evolution of porosity is of relevance for assessing damage during both quasi-static and high strain-rate deformation of metallic aggregates. The Gurson (1977) criterion, which provides a constitutive relation between yield stress and strain-rate in voided materials, is widely used in simulations of metal deformation under complex boundary conditions (e.g., Johnson and Addessio, 1988). The Gurson constitutive law follows from an upper-bound solution of a unit cell problem, based on the simplifying

---

* Corresponding author. Tel.: +1-505-6650892; fax: +1-505-6678021.
E-mail addresses: ricardo@ifir.edu.ar (R.A. Lebensohn), tome@lanl.gov (C.N. Tomé).

Nomenclature

(*a*) *Velocities, stresses and strain-rates*

$\dot{u}_i(\bar{x}), \dot{u}_{i,j}(\bar{x})$ — velocity and velocity-gradient fields.

$\dot{\varepsilon}_{ij}(\bar{x}), \dot{\varepsilon}_{ij}, \dot{E}_{ij}$ — strain-rate field, average strain-rate in each grain and macroscopic strain-rate.

$\sigma_{ij}(\bar{x}), \sigma_{ij}, \Sigma_{ij}$ — Cauchy stress (field, average in each grain, and macroscopic).

$\dot{\varepsilon}_{ij}^{\mathrm{d}}(\bar{x}), \dot{\varepsilon}_{ij}^{\mathrm{d}}, \dot{E}_{ij}^{\mathrm{d}}$ — deviatoric strain-rate (field, average in each grain, and macroscopic).

$\dot{\varepsilon}^{\mathrm{s}}(\bar{x}) = \mathrm{tr}\,\dot{\varepsilon}_{ij}(\bar{x}), \dot{\varepsilon}^{\mathrm{s}} = \mathrm{tr}\,\dot{\varepsilon}_{ij},$
$\dot{E}^{\mathrm{s}} = \mathrm{tr}\,\dot{E}_{ij}$ — dilatation-rate (field, average in each grain, and macroscopic).

$\sigma_{ij}^{\mathrm{d}}(\bar{x}), \sigma_{ij}^{\mathrm{d}}, \Sigma_{ij}^{\mathrm{d}}$ — deviatoric stress (field, average in each grain, and macroscopic).

$\sigma^{\mathrm{s}}(\bar{x}) = \frac{1}{3}\,\mathrm{tr}\,\sigma_{ij}(\bar{x}), \ \ \sigma^{\mathrm{s}} = \frac{1}{3}\,\mathrm{tr}\,\sigma_{ij},$
$\Sigma^{\mathrm{s}} = \frac{1}{3}\,\mathrm{tr}\,\Sigma_{ij}$ — mean stress (field, average in each grain, and macroscopic).

$\tilde{u}_i(\bar{x})$ — local deviation of the velocity field from macroscopic velocity field.

$\tilde{\dot{\varepsilon}}_{ij}^{\mathrm{d}}(\bar{x}) = \dot{\varepsilon}_{ij}^{\mathrm{d}}(\bar{x}) - \dot{E}_{ij}^{\mathrm{d}}, \tilde{\dot{\varepsilon}}_{ij}^{\mathrm{d}} = \dot{\varepsilon}_{ij}^{\mathrm{d}} - \dot{E}_{ij}^{\mathrm{d}}$ — local deviation of deviatoric strain-rate (field and average in each grain).

$\tilde{\dot{\varepsilon}}^{\mathrm{s}}(\bar{x}) = \dot{\varepsilon}^{\mathrm{s}}(\bar{x}) - \dot{E}^{\mathrm{s}}, \tilde{\dot{\varepsilon}}^{\mathrm{s}} = \dot{\varepsilon}^{\mathrm{s}} - \dot{E}^{\mathrm{s}}$ — local deviation of dilatation-rate (field and average in each grain).

$\tilde{\sigma}_{ij}^{\mathrm{d}}(\bar{x}) = \sigma_{ij}^{\mathrm{d}}(\bar{x}) - \Sigma_{ij}^{\mathrm{d}}, \tilde{\sigma}_{ij}^{\mathrm{d}} = \sigma_{ij}^{\mathrm{d}} - \Sigma_{ij}^{\mathrm{d}}$ — local deviation of deviatoric stress (field and average in each grain).

$\tilde{\sigma}^{\mathrm{s}}(\bar{x}) = \sigma^{\mathrm{s}}(\bar{x}) - \Sigma^{\mathrm{s}}, \tilde{\tilde{\varepsilon}}^{\mathrm{s}} = \sigma^{\mathrm{s}} - \Sigma^{\mathrm{s}}$ — local deviation of mean stress (field and average in each grain).

(*b*) *Moduli*

$M_{ijkl}, \bar{M}_{ijkl}$ — viscoplastic compliance (in each grain and macroscopic).

$\dot{\varepsilon}_{ij}^{\mathrm{do}}, \dot{E}_{ij}^{\mathrm{do}}$ — back-extrapolated term (in each grain and macroscopic).

$L_{ijkl}, \bar{L}_{ijkl}$ — viscoplastic stiffness (in each grain and macroscopic).

$K, \bar{K}$ — viscoplastic bulk modulus (in each grain and macroscopic).

(*c*) *Green and Eshelby tensors and scalars*

$\dot{\varepsilon}_{ij}^{\mathrm{d}*}(\bar{x}), \dot{\varepsilon}_{ij}^{\mathrm{d}*}$ — deviatoric eigen-strain-rate (field and average in each grain).

$\dot{\varepsilon}^{\mathrm{s}*}(\bar{x}), \dot{\varepsilon}^{\mathrm{s}*}$ — eigen-dilatation-rate (field and average in each grain).

$\tilde{u}^{\mathrm{d}}_{i,j}(\bar{x}), \tilde{u}^{\mathrm{d}}_{i,j}$	contribution of deviatoric components to local deviation of velocity-gradient (field and average in the grain).
$\tilde{u}^{\mathrm{s}}_{i,j}(\bar{x}), \tilde{u}^{\mathrm{s}}_{i,j}$	contribution of spherical components to local deviation of velocity-gradient (field and average in the grain).
$T^{\mathrm{d}}_{ijkl}, T^{\mathrm{s}}_{ij}$	deviatoric and spherical Green interaction tensors.
$S^{\mathrm{d}}_{ijkl}, S^{\mathrm{s}}_{ij}$	deviatoric and spherical Eshelby tensors.
$\Psi = \mathrm{tr}(S^{\mathrm{s}}_{ij})$	Eshelby factor (trace of spherical Eshelby tensor)
(d) Interaction and localization tensors and factors	
$\tilde{M}_{ijkl}, \tilde{\beta}_{kl}, \tilde{K}$	deviatoric and coupling interaction tensors and spherical interaction factor.
$B_{ijkl}, \Phi_{ij}, B^{\mathrm{s}}$	stress localization tensors and factor
$A_{ijkl}, \Omega_{ij}, A^{\mathrm{s}}$	strain-rate localization tensors and factor

assumptions of: elastically rigid, isotropic perfectly plastic, rate-independent matrix plastic behavior, spherical voids, and no void interaction. Such assumptions do not adequately represent many situations in which the anisotropy of the material response, and/or the void shape, and/or rate effects may play a role. As a consequence, modifications of the Gurson model have been proposed to address some of these issues, e.g: void shape (Lee and Mear, 1991; Golaganu et al., 1993, 1994; Garajeu et al., 2000), matrix anisotropy (Chen et al., 2000), rate-sensitivity (Lee and Mear, 1991; Addessio and Johnson, 1993; Garajeu et al., 2000; Liu et al., 2000; Chen et al., 2002) and void interaction (Tvergaard, 1982; Garajeu et al., 2000).

Ponte Castañeda and coworkers (Ponte Castañeda and Zaidman, 1996; Kailasam et al., 1997a, b), on the other hand, have developed a model based on the variational formulation of Ponte Castañeda (1991), to predict the behavior of porous rate-sensitive materials with isotropic phases, taking into account the field fluctuations induced by the presence of voids and the anisotropy induced by void shape evolution. The best performance of this model is obtained at low void concentration and low triaxiality. Such formulation was implemented inside an elastoplastic FEM code to account for the evolution of porosity and the development of anisotropy due to changes in the shape and orientation of the voids during deformation (Kailasam et al., 2000). Later, Ponte Castañeda (1996) developed a second variational formulation that yields estimates that are exact to second-order in the fluctuation of properties between phases, therefore specially suitable for porous materials. This second-order procedure, however, does not take into account the field fluctuations and therefore is not accurate for cases near percolation and/or of high triaxiality. More recently, Ponte Castañeda (2002a, b) developed a new formulation that combines the main advantages of the former models (i.e., takes into account the field fluctuations and is exact to second-order in the contrast) which can be applied to the high triaxiality and void concentration case.

The study of the interplay between texture and anisotropy of polycrystalline materials motivated the development of numerous polycrystal models. Such models allow us to predict the evolution of anisotropy, texture and hardening during plastic deformation of an aggregate of anisotropic grains. When the single crystal anisotropy is severe, selfconsistent formulations should be used, instead of the simpler upper-bound formulation (Taylor, 1938), to obtain accurate results. In particular, the fully anisotropic visco-plastic self-consistent (VPSC) model developed by Lebensohn and Tomé (1993), based on the original Molinari et al. (1987) isotropic formulation, has been successfully used in the last ten years to describe the constitutive response of a variety of anisotropic systems under diverse loading conditions. Recently, VPSC has been interfaced with FEM codes to describe the forming of Zr and Zr alloys (Logé et al., 1998; Tomé et al., 2001) under complex boundary conditions.

Although the VPSC polycrystal theories have also been extended to multiphase polycrystals (e.g., Lebensohn and Canova, 1997) no model until now was available to treat the large-strain deformation of voided polycrystals, i.e. an extreme case of a two-phase aggregate with infinite contrast between phases. A formulation with such characteristics would be useful, for example, to predict the behavior of anisotropic materials subjected to dynamic loading conditions, with the ultimate goal of building a numerical interface with dynamic FEM codes. With this in mind, we present here a 3D VPSC model for polycrystals with prexisting voids, which allows us to consider the full anisotropy associated with morphologic evolution of voids and grains and with crystallographic texture development in the aggregate, as well as rate effects. The model applies to the stage of void growth but not to the previous stage of void nucleation nor the subsequent stage of void coalescence.

The formulation is a generalization of the incompressible fully anisotropic VPSC model of Lebensohn and Tomé (1993) and Lebensohn et al. (1998). This model treats each grain as a viscoplastic ellipsoidal inclusion embedded in a Homogeneous Effective Medium (HEM). Since both the inclusion and the HEM are anisotropic and incompressible, the model was formulated in the deviatoric five-dimensional space. In the present extension, cavities are still treated as ellipsoidal inclusions, but the assumption of incompressibility applies neither to the voids nor to the HEM (the inclusions representing grains, however, remain incompressible). Dilatation and hydrostatic pressure have to be accounted for, and they represent the sixth dimension of the problem.

An important requirement for this extended VPSC formulation is that it should reproduce Gurson's results for the case of rate-insensitive isotropic aggregates with spherical voids, for different triaxialities and porosities. The procedure used here for adjusting the extended VPSC formulation to the Gurson limit is inspired by the work of Ponte Castañeda (2002a, b), and is based on adjusting the local linearized behavior in the grains to implicitly take into account the field fluctuations in the grains due to the presence of voids. To accomplish this, it has been necessary to generalize the tangent VPSC model of Lebensohn and Tomé (1993) to allow for an ad-hoc linearization of the grain's constitutive response, as originally proposed by Masson et al. (2000) in their affine formulation.

In the next section we describe the formulation and discuss its assumptions (due to space limitations we have omitted a detailed derivation of some equations of the

formulation which can be found in the report by Lebensohn et al., 2003). Next we illustrate some of the capabilities of the model with several applications. First we make a comparison with Gurson model, after which we study the role of texture, rate-sensitivity, and void morphology (shape) upon porosity evolution and stress–strain response. We consider both fcc and hcp polycrystals in this analysis.

2. Extended VPSC model

2.1. Local constitutive behavior and homogenization

Let us consider an aggregate consisting of grains (material phase) and cavities (void phase). The deviatoric part of the viscoplastic constitutive behavior of the material phase at local level is described by means of the non-linear rate-sensitivity equation:

$$\dot{\varepsilon}_{ij}^{\mathrm{d}}(\bar{x}) = \dot{\gamma}_{\mathrm{o}} \sum_s m_{ij}^{\mathrm{s}}(\bar{x}) \left(\frac{m_{kl}^{\mathrm{s}}(\bar{x})\sigma_{kl}^{\mathrm{d}}(\bar{x})}{\tau^{\mathrm{s}}(\bar{x})} \right)^n, \tag{1}$$

where $\dot{\varepsilon}_{ij}^{\mathrm{d}}(\bar{x})$ and $\sigma_{kl}^{\mathrm{d}}(\bar{x})$ are the deviatoric strain-rate and stress fields; $m_{ij}^{\mathrm{s}}(\bar{x})$ and $\tau^{\mathrm{s}}(\bar{x})$ are the Schmid tensor and the threshold stress of slip (s); $\dot{\gamma}_{\mathrm{o}}$ is a normalization factor and n is the rate-sensitivity exponent. Linearizing Eq. (1) inside the domain of a grain and adding a linear relation between the spherical components of stress and strain-rate gives

$$\dot{\varepsilon}_{ij}^{\mathrm{d}}(\bar{x}) = M_{ijkl}\sigma_{kl}^{\mathrm{d}}(\bar{x}) + \dot{\varepsilon}_{ij}^{\mathrm{do}}, \tag{2a}$$

$$\dot{\varepsilon}^{\mathrm{s}}(\bar{x}) = K^{-1}\sigma^{\mathrm{s}}(\bar{x}), \tag{2b}$$

where $\dot{\varepsilon}^{\mathrm{s}}(\bar{x}) = \mathrm{tr}\,\dot{\varepsilon}_{ij}(\bar{x})$ and $\sigma^{\mathrm{s}}(\bar{x}) = \frac{1}{3}\,\mathrm{tr}\,\sigma_{ij}(\bar{x})$ are the spherical components of the local fields; $M_{ijkl}, \dot{\varepsilon}_{ij}^{\mathrm{do}}$ and K are the grain's viscoplastic compliance, back extrapolated term, and viscoplastic bulk modulus, respectively. Concerning the linearization in the equation that relates the deviatoric components in the material phase, M_{ijkl} and $\dot{\varepsilon}_{ij}^{\mathrm{do}}$ can be chosen differently. While the original VPSC formulation (Molinari et al., 1987; Lebensohn and Tomé, 1993) was restricted to the assumption of a tangent linearization of the local behavior, Masson et al. (2000) generalized these kinds of selfconsistent formulations to arbitrary linearized behaviors, by means of the so-called affine procedure. In what follows, we will adopt Masson et al.'s affine linearization scheme, since it provides the required flexibility to take into account the effect of porosity on the local behavior of the material phase, leaving for later the discussion of which is the best choice of the linear moduli, in the case of voided polycrystals.

In what concerns the equation that relates the spherical components, it expands the scope of the constitutive response, and the derivation that follows is general and has application beyond the specific case of voided polycrystals. For the grains of an incompressible solid phase it holds that $K \to \infty$, and Eq. (2b) just states the condition of incompressibility. In such case, solving simultaneously Eqs. (2a) and (2b) allowed

us (Lebensohn et al., 1998) to solve the problem of the incompressible inclusion with no need of using the "penalty method", which consists in assuming a very small (rather than null) compressibility (Hutchinson, 1976). As for the infinitely compliant void phase, we can write expressions formally equivalent to (2), taking $M_{ijkl} \to \infty$ and $K = 0$.

Performing homogenization on this heterogeneous medium consists in assuming pseudo-linear constitutive relations analogous to (2) at the effective medium (polycrystal) level:

$$\dot{E}_{ij}^{d} = \bar{M}_{ijkl} \Sigma_{kl}^{d} + \dot{E}_{ij}^{do}, \tag{3a}$$

$$\dot{E}^{s} = \bar{K}^{-1} \Sigma^{s}, \tag{3b}$$

where $\dot{E}_{ij}^{d}$, Σ_{ij}^{d}, $\dot{E}^{s}$ and Σ^{s} are overall (macroscopic) deviatoric and spherical magnitudes and $\bar{M}_{ijkl}$, $\dot{E}_{ij}^{do}$ and $\bar{K}$ are the macroscopic viscoplastic compliance, back extrapolated term and viscoplastic bulk modulus, respectively. The latter moduli are unknown a priori and should be adjusted self-consistently. Due to the presence of voids, the effective viscoplastic bulk modulus $\bar{K}$ has a finite non-zero value, even if the solid material is incompressible. Invoking the concept of the equivalent inclusion (Mura, 1988), the local constitutive behavior can be rewritten in terms of the homogeneous macroscopic moduli, so that the inhomogeneity is hidden inside a fictitious eigen-strain-rate, as

$$\dot{\varepsilon}_{ij}^{d}(\bar{x}) = \bar{M}_{ijkl} \sigma_{kl}^{d}(\bar{x}) + \dot{E}_{ij}^{do} + \dot{\varepsilon}_{ij}^{d*}(\bar{x}), \tag{4a}$$

$$\dot{\varepsilon}^{s}(\bar{x}) = \bar{K}^{-1} \sigma^{s}(\bar{x}) + \dot{\varepsilon}^{s*}(\bar{x}), \tag{4b}$$

where $\dot{\varepsilon}_{ij}^{d*}(\bar{x})$ and $\dot{\varepsilon}^{s*}(\bar{x})$ are the deviatoric eigen-strain-rate field and a newly defined eigen-dilatation-rate field, respectively, which follow from replacing the inhomogeneity by an equivalent inclusion. Rearranging and subtracting (3) from (4) gives

$$\tilde{\dot{\sigma}}_{ij}^{d}(\bar{x}) = \bar{L}_{ijkl}(\tilde{\dot{\varepsilon}}_{kl}^{d}(\bar{x}) - \dot{\varepsilon}_{kl}^{d*}(\bar{x})), \tag{5a}$$

$$\tilde{\dot{\sigma}}^{s}(\bar{x}) = \bar{K}(\tilde{\dot{\varepsilon}}^{s}(\bar{x}) - \dot{\varepsilon}^{s*}(\bar{x})), \tag{5b}$$

where the "$\sim$" quantities are local deviations from macroscopic values and $\bar{L}_{ijkl} = \bar{M}_{ijkl}^{-1}$. Combining (5) with the equilibrium condition:

$$\sigma_{ij,j}(\bar{x}) = \tilde{\sigma}_{ij,j}(\bar{x}) = \tilde{\sigma}_{ij,j}^{d}(\bar{x}) + \tilde{\sigma}_{,i}^{s}(\bar{x}) \tag{6}$$

and using the relation between strain-rate and velocity-gradient, i.e. $\tilde{\dot{\varepsilon}}_{ij}(\bar{x}) = \frac{1}{2}(\tilde{\dot{u}}_{i,j}(\bar{x}) + \tilde{\dot{u}}_{j,i}(\bar{x}))$, we obtain

$$\bar{L}_{ijkl}\tilde{\dot{u}}_{k,lj}(\bar{x}) + \tilde{\dot{\sigma}}_{,i}^{s}(\bar{x}) + f_{i}^{d}(\bar{x}) = 0, \tag{7a}$$

$$\bar{K}\tilde{\dot{u}}_{k,k}(\bar{x}) - \tilde{\dot{\sigma}}^{s}(\bar{x}) + f^{s}(\bar{x}) = 0, \tag{7b}$$

where the fictitious forces associated with the heterogeneity are

$$f_i^d(\bar{x}) = -\bar{L}_{ijkl}\dot{\varepsilon}_{kl,j}^{d*}(\bar{x}) = \sigma_{ij,j}^{d*}(\bar{x}), \tag{8}$$

$$f^s(\bar{x}) = -\bar{K}\dot{\varepsilon}^{s*}(\bar{x}), \tag{9}$$

2.2. Integration of equations—Eshelby tensors and factors

System (7) consists of four differential equations with four unknowns: three are the components of the velocity deviation vector $\tilde{u}_i(\bar{x})$, and one is the mean stress deviation $\tilde{\sigma}^s(\bar{x})$. The solution of such system using Green functions and Fourier transforms leads to the following expression for the average strain-rate deviation inside the inclusion (see Appendix):

$$\tilde{\dot{u}}_{k,l} = T_{klij}^d \bar{L}_{ijmn}\dot{\varepsilon}_{mn}^{d*} + T_{kl}^s\dot{\varepsilon}^{s*}, \tag{10}$$

where T_{klij}^d and T_{kl}^s are the deviatoric and spherical Green interaction tensors, given by Eqs. (A.10)–(A.11). It is convenient to define a fourth order "deviatoric" and a second order "spherical" symmetric Eshelby tensor as

$$S_{ijkl}^d = \frac{1}{4}(T_{ijmn}^d + T_{jimn}^d + T_{ijnm}^d + T_{jinm}^d)\bar{L}_{mnkl}, \tag{11}$$

$$S_{ij}^s = \frac{1}{2}(T_{ij}^s + T_{ji}^s). \tag{12}$$

Taking the symmetric part of (10) and using (11) and (12), we obtain the strain-rate deviation in the inclusion:

$$\tilde{\dot{\varepsilon}}_{ij} = S_{ijkl}^d\dot{\varepsilon}_{kl}^{d*} + S_{ij}^s\dot{\varepsilon}^{s*}. \tag{13}$$

The deviator and the trace of $\tilde{\dot{\varepsilon}}_{ij}$ are

$$\tilde{\dot{\varepsilon}}_{ij}^d = S_{ijmn}^d\dot{\varepsilon}_{mn}^{d*} + S_{ij}^s\dot{\varepsilon}^{s*} - \frac{1}{3}\delta_{ij}\tilde{\dot{\varepsilon}}^s, \tag{14}$$

$$\tilde{\dot{\varepsilon}}^s = S_{kkmn}^d\dot{\varepsilon}_{mn}^{d*} + \Psi\dot{\varepsilon}^{s*}, \tag{15}$$

where $\Psi = \mathrm{tr}(S_{ij}^s)$ will be called in what follows the "spherical Eshelby factor". At this point we need to find the deviatoric and spherical eigen-strain-rates. From (15) we have

$$\dot{\varepsilon}^{s*} = \frac{\tilde{\dot{\varepsilon}}^s}{\Psi} - \frac{S_{kkmn}^d}{\Psi}\dot{\varepsilon}_{mn}^{d*}. \tag{16}$$

Replacing (16) inside (14):

$$\tilde{\dot{\varepsilon}}_{ij}^d = (S_{ijmn}^d - \xi_{ijmn})\dot{\varepsilon}_{mn}^{d*} + \beta_{ij}\tilde{\dot{\varepsilon}}^s, \tag{17}$$

where

$$\beta_{ij} = \frac{S^s_{ij}}{\text{tr}(S^s_{ij})} - \frac{\delta_{ij}}{3}, \tag{18}$$

$$\xi_{ijmn} = \frac{S^s_{ij}S^d_{kkmn}}{\Psi}. \tag{19}$$

According to (17), β_{ij} describes the coupling between the spherical and the deviatoric components of the strain-rate. For this reason, it will be called here: "Eshelby coupling tensor". Furthermore, using symmetry considerations, it is easy to realize that (18) would vanish in the case of a spherical inclusion embedded in an isotropic matrix. As a consequence, β_{ij} can be interpreted as a measure of the anisotropy of the medium, and the deviatoric-spherical coupling can be expected to become stronger as the anisotropy of the medium increases or to vanish if the medium is isotropic. The latter situation, however, is never found if the material's behavior is non-linear (i.e., $n \neq 1$ in Eq. (1)). In such a case, even if the polycrystal has a random texture, the viscoplastic compliance tensor is a function of the stress state and the response of the homogeneous medium will be, in general, anisotropic, resulting in a non-vanishing β_{ij} tensor. On the other hand, in what concerns ξ_{ijmn}, we have checked numerically (Lebensohn et al., 2003) that the norm of ξ_{ijmn} is, for our purposes, at least two orders of magnitude smaller than the norm of S^d_{ijmn}, and can be neglected. Then, the following approximation holds:

$$\tilde{\dot{\varepsilon}}^d_{ij} \cong S^d_{ijmn}\dot{\varepsilon}^{d*}_{mn} + \beta_{ij}\tilde{\dot{\varepsilon}}^s \tag{20}$$

from where the deviatoric eigen-strain-rate $\dot{\varepsilon}^{d*}_{mn}$ is obtained as

$$\dot{\varepsilon}^{d*}_{mn} = S^{d^{-1}}_{mnpq}(\tilde{\dot{\varepsilon}}^d_{pq} - \beta_{pq}\tilde{\dot{\varepsilon}}^s). \tag{21}$$

Replacing (21) in (16) it can be proved, using $S^d_{kkmn}S^{d^{-1}}_{mnpq} = \delta_{kp}\delta_{kq}$, $\text{tr}\,\tilde{\dot{\varepsilon}}^d_{ij} = 0$, and $\text{tr}\,\beta_{ij} = 0$, that

$$\dot{\varepsilon}^{s*} = \frac{\tilde{\dot{\varepsilon}}^s}{\Psi}. \tag{22}$$

Eq. (21) indicates that the deviatoric strain-rate is coupled to both the deviatoric eigen-strain-rate and the eigen-dilatation-rate, while (22) shows that, under the assumption (20), the dilatation-rate depends only on the eigen-dilatation-rate.

2.3. Interaction and localization equations

The local constitutive behavior Eq. (2) also describes the relation between the average stress and strain-rate in the domain of the grains and expressions similar to Eqs. (5), relating deviations with respect to overall quantities, also hold for the average

stress, strain-rate, and eigen-strain-rates in the grains:

$$\tilde{\sigma}_{ij}^{d} = \bar{L}_{ijkl}(\tilde{\dot{\varepsilon}}_{kl}^{d} - \dot{\varepsilon}_{kl}^{d*}), \tag{23a}$$

$$\tilde{\sigma}^{s} = \bar{K}(\tilde{\dot{\varepsilon}}^{s} - \dot{\varepsilon}^{s*}). \tag{23b}$$

Replacing the expressions (21) and (22) that give the eigen-strain-rates in terms of the strain-rate deviations into the deviation equations (23), we obtain the following interaction equations:

$$\tilde{\dot{\varepsilon}}_{ij}^{d} = -\tilde{M}_{ijkl}\tilde{\sigma}_{kl}^{d} - \tilde{\beta}_{kl}\tilde{\sigma}^{s}, \tag{24a}$$

$$\tilde{\dot{\varepsilon}}^{s} = -(1/\tilde{K})\tilde{\sigma}^{s}, \tag{24b}$$

where the interaction tensors and factor are given by

$$\tilde{M}_{ijkl} = (I - S^{d})_{ijmn}^{-1}S_{mnpq}^{d}\bar{M}_{pqkl}, \tag{25a}$$

$$\tilde{\beta}_{ij} = (1/\tilde{K})(I - S^{d})_{ijmn}^{-1}\beta_{mn}, \tag{25b}$$

$$\tilde{K} = \frac{1 - \Psi}{\Psi}\bar{K}. \tag{25c}$$

Replacing the local and overall deviatoric constitutive relations into the interaction equations (24) we can write, after some manipulation, the following localization equations for the deviatoric and spherical stress components:

$$\sigma_{ij}^{d} = B_{ijkl}\Sigma_{kl}^{d} + \Phi_{ij}, \tag{26a}$$

$$\sigma^{s} = B^{s}\Sigma^{s}, \tag{26b}$$

where the localization tensors are defined as

$$B_{ijkl} = (M + \tilde{M})_{ijmn}^{-1}(\bar{M} + \tilde{M})_{mnkl}, \tag{27a}$$

$$\Phi_{ij} = (M + \tilde{M})_{ijkl}^{-1}(\dot{E}_{kl}^{do} - \dot{\varepsilon}_{kl}^{do} - \tilde{\beta}_{kl}\tilde{\sigma}^{s}), \tag{27b}$$

$$B^{s} = \frac{K}{\bar{K}}\frac{\bar{K} + \tilde{K}}{K + \tilde{K}}. \tag{27c}$$

For a solid phase ($K \rightarrow \infty$) the limit of Eq. (27c) is well defined. In the case of a void phase, for which $L_{ijkl} = 0$, $M_{ijkl} \rightarrow \infty$, and $K = 0$, the localization tensors become null tensors:

$$B_{ijkl} = 0, \quad \Phi_{ij} = 0, \quad B^{s} = 0, \tag{28}$$

which is to be expected, since a void cannot sustain stress. However, the void does contribute to strain. As a consequence, we need to derive alternative localization equations in terms of strain-rates. Inverting the local and overall constitutive equations, and expressing them in terms of stiffness tensors (i.e., $L_{ijkl} = M_{ijkl}^{-1}$, $\bar{L}_{ijkl} = \bar{M}_{ijkl}^{-1}$ and $\tilde{L}_{ijkl} = \tilde{M}_{ijkl}^{-1}$) and following a similar procedure, we obtain the localization relation for the strain-rate components:

$$\dot{\varepsilon}_{ij}^{\mathrm{d}} = A_{ijkl}\dot{E}_{kl}^{\mathrm{d}} + \Omega_{ij}, \tag{29a}$$

$$\dot{\varepsilon}^{\mathrm{s}} = A^{\mathrm{s}}\dot{E}^{\mathrm{s}}. \tag{29b}$$

For the solid phase ($K \to \infty$) the localization tensors are

$$A_{ijkl} = (L + \tilde{L})_{ijmn}^{-1}(\bar{L} + \tilde{L})_{mnkl}, \tag{30a}$$

$$\Omega_{ij} = (L + \tilde{L})_{ijkl}^{-1}(-\bar{L}:\dot{E}^{\mathrm{do}} + L:\dot{\varepsilon}^{\mathrm{do}} - \tilde{L}:\tilde{\beta}\tilde{\sigma}^{\mathrm{s}})_{kl}, \tag{30b}$$

$$A^{\mathrm{s}} = \frac{\bar{K} + \tilde{K}}{K + \tilde{K}} = 0, \tag{30c}$$

while for the void phase ($K = 0$) they are

$$A_{ijkl} = I_{ijkl} + \tilde{L}_{ijmn}^{-1}L_{mnkl}, \tag{31a}$$

$$\Omega_{ij} = -\tilde{L}_{ijkl}^{-1}L_{klmn}\dot{E}_{mn}^{\mathrm{do}} - \tilde{\beta}_{ij}\tilde{\sigma}^{\mathrm{s}}, \tag{31b}$$

$$A^{\mathrm{s}} = \frac{\bar{K} + \tilde{K}}{\tilde{K}}. \tag{31c}$$

2.4. Self-consistent polycrystal model

The derivation presented in the previous sections solves the problem of a viscoplastic compressible inclusion embedded in a viscoplastic compressible effective medium being subject to external loading conditions. In this section we are going to use the previous result to construct a polycrystal model that regards each grain as an ellipsoidal inclusion embedded in an effective medium which represents the polycrystal. The properties of such medium are not known a priori but have to be found thorough an iterative self-consistent procedure. Replacing the stress localization equations in the local constitutive equations, enforcing the condition that the weighted average of the strain-rate over the aggregate has to coincide with the macroscopic quantities and using the macroscopic constitutive equations (Lebensohn et al., 2003), we obtain the following self-consistent equations for the homogeneous compliances and back-extrapolated term:

$$\bar{M}_{ijmn} = \langle M_{ijkl}B_{klmn}\rangle, \tag{32a}$$

$$\dot{E}_{ij}^{\mathrm{do}} = \langle M_{ijkl}\Phi_{kl} + \dot{\varepsilon}_{ij}^{\mathrm{do}}\rangle, \tag{32b}$$

$$\bar{K} = \langle K^{-1}B^{\mathrm{s}}\rangle^{-1}. \tag{32c}$$

When the averages in (32) have to be evaluated for the void phase (in which case $M_{ijkl} \to \infty$, $B_{ijkl}=0$ and $\Phi_{ij}=0$) the following identities are specially useful (Lebensohn et al., 2003):

$$M_{ijkl}B_{klmn} = A_{ijkl}\bar{M}_{klmn}, \tag{33a}$$

$$M_{ijkl}\Phi_{kl} + \dot{\varepsilon}_{ij}^{\mathrm{do}} = A_{ijkl}\dot{E}_{kl}^{\mathrm{do}} + \Omega_{ij}. \tag{33b}$$

If the shape of the grains and the voids is the same, then the Eshelby factor Ψ, and therefore $\tilde{K}$ (given by Eq. (25c)), are unique. In such a case (32c) gives the following self-consistent equation for the effective bulk modulus:

$$\bar{K} = \left\langle \frac{K}{K + \tilde{K}} \right\rangle (\bar{K} + \tilde{K}). \tag{34}$$

Since $K \to \infty$ for the incompressible material phase, and $K = 0$ for the void phase, it holds that

$$\frac{K}{K + \tilde{K}} = \begin{vmatrix} 1 & \text{for grains,} \\ 0 & \text{for voids.} \end{vmatrix} \tag{35}$$

Then, the self-consistent equation for the viscoplastic bulk modulus is given by

$$\bar{K} = \frac{1 - \phi}{\Psi} \tilde{K}, \tag{36}$$

where ϕ is the current porosity (relative volume fraction of voids) in the polycrystal.

The self-consistent equations (32) are derived imposing the average of the local strain-rates to coincide with the applied macroscopic strain-rate. It can be shown (Lebensohn et al., 2003) that these equations are also consistent with the condition that the average of the local stresses coincide with the macroscopic stress only if the shape of all inclusions (grains and voids) is unique. If the grains and the voids have each a different shape, they have associated different Eshelby tensors and factors, and consequently the interaction tensors cannot be factored from the averages. In this case, a generalized self-consistent method should be used (Walpole, 1969; Lebensohn et al., 1996) which gives the following extended relations:

$$\bar{M}_{ijkl} = \langle M : B \rangle_{ijmn} \langle B \rangle_{mnkl}^{-1}, \tag{37a}$$

$$\dot{E}_{ij}^{\mathrm{do}} = \langle M : \Phi + \dot{\varepsilon}^{\mathrm{do}} \rangle_{ij} - \langle M : B \rangle_{ijkl} \langle B \rangle_{klmn}^{-1} \langle \Phi \rangle_{mn}, \tag{37b}$$

$$\bar{K} = \frac{1 - \phi}{\phi} \frac{1 - \Psi_v}{\Psi_g} \tilde{K}, \tag{37c}$$

where Ψ_g and Ψ_v are the traces of the spherical Eshelby tensors associated with the grains and the voids, respectively. In writing (37c) we assume that all the grains and all the voids have the same shape (although different from each other's). The derivation of expressions (37) can be found elsewhere (Lebensohn et al., 2003). The self-consistent equations (32) are a particular case of (37). Both sets constitute fixed-point equations that provide improved estimates of $\bar{M}_{ijkl}, \dot{E}_{ij}^{\mathrm{do}}$ and $\bar{K}$, when they are solved iteratively starting from an initial guess for the latter tensors. From a numerical point of view,

Eqs. (37) are more robust and improve the speed and stability of the convergence procedure, even when solving a problem where all the inclusions have the same shape.

2.5. Local linearization for voided polycrystals

As stated earlier, the deviatoric local constitutive behavior (Eq. (2a)) can be linearized in different ways, and the macroscopic response resulting from the selfconsistent formulation will depend on the choice made for that linearization. For instance, if the back-extrapolated term $\dot{\varepsilon}_{ij}^{do}$ is a priori set to zero, the resulting model is a secant one, which has been proved to be in general too stiff, leading to close-to-upper-bound results. On the other hand, if $M_{ijkl} = \partial \dot{\varepsilon}_{ij}^{d}(\sigma_{ij}^{d})/\partial \sigma_{kl}^{d}$, the model is tangent (Molinari et al., 1987; Lebensohn and Tomé, 1993), and gives a more compliant response. However, as pointed out by Ponte Castañeda (2002a), any homogenization scheme whose local linearization depends only on the average of local states in the phases (or grains) fails in reproducing Gurson's results at high triaxialities, and leads to a completely rigid response in the pure hydrostatic limit. This result is connected to the high deformation gradients that physically exist inside the phases (or grains), in the vicinity of a void, when high hydrostatic pressure is applied to the aggregate. Linearizing a power law using the tangent at the mid-point (first order moment) of the intragranular stress distribution underestimates, in general, all the rates within the interval. But, in particular, the rates at the higher stresses, which make the effective response of the phases (grains) softer, can be seriously underestimated. In fact, Suquet (1995) showed that estimating the magnitudes of the intraphase (intragranular) fluctuations (second order moments) and linearizing the local behavior in terms of them, rather than just using the average states, softens the predicted effective behavior of the aggregate. For these reasons, good matching between the present theory (in its isotropic and rate-insensitive limit) and the Gurson model at high triaxialities requires to generalize the linearization. We define the slope of the local compliance as

$$M_{ijkl}(\hat{\sigma}_{kl}^{d} - \sigma_{kl}^{d}) = (\hat{\dot{\varepsilon}}_{ij}^{d} - \dot{\varepsilon}_{ij}^{d}). \tag{38}$$

Here, σ_{kl}^{d} is the average stress in the grain. As for $\hat{\sigma}_{kl}^{d}$ we propose an empirical functional form, colinear with σ_{kl}^{d}:

$$\hat{\sigma}_{kl}^{d} = (1 + \alpha(X, \phi) \times |X|)\sigma_{kl}^{d}. \tag{39}$$

Here $X = \Sigma^{s}/\Sigma^{d}$ is the stress triaxiality (to be called triaxiality in what follows). Σ^{s} is the macroscopic hydrostatic pressure, $\Sigma^{d} = (3/2\Sigma_{ij}^{d}\Sigma_{ij}^{d})^{1/2}$ is the macroscopic equivalent deviatoric (Von Mises) stress, and $\alpha(X, \phi)$ is an empirical "super-tangent" parameter whose dependence with X and ϕ is adjusted to match the predictions of Gurson's formulation for an isotropic and rate-insensitive polycrystal. Defined in this way, the local tensors $\hat{\sigma}_{kl}^{d}$ are evidently related with the stress fluctuations. Here, rather than estimate them directly, we fit the parameter $\alpha(X, \phi)$ to the Gurson model for different triaxialities and porosities. Observe that by setting $\alpha = 0$ the tangent formulation is recovered, while $\alpha < 0$ corresponds to a stiffer-than-tangent approximation, closer to the secant response.

2.6. Fitting of $\alpha(X, \phi)$ using the Gurson model

The Gurson (1977) model follows from solving the localization problem on a representative volume element formed by the solid phase and a void included at the center. The assumptions of the model are that the solid phase is isotropic rigid-plastic (with an effective yield stress Y) and rate-insensitive, and that the void is spherical. Under such conditions the effective yield stress for the effective medium is

$$\Sigma^d = Y\sqrt{1 + \phi^2 - 2\phi \cosh\left(\frac{3\Sigma^s}{2Y}\right)}. \tag{40}$$

Eq. (40) describes a yield surface in the 3D space defined by the normalized stresses $\Sigma^d/Y, \Sigma^s/Y$, and the porosity ϕ. Such a yield surface defines, for a given porosity, the stress state that fulfills the yield condition. This equation depends on the hydrostatic pressure and reduces to the classical Von Mises yield condition when the porosity is null. When the spherical stress component is zero, Eq. (40) predicts a yield stress corrected for the porosity, i.e.

$$\Sigma^d = Y(1 - \phi). \tag{41}$$

When the deviatoric stress component is zero this expression leads to the Carroll and Holt (1972) limit:

$$\Sigma^s = 2/3 \, Y \ln(1/\phi). \tag{42}$$

Eq. (42) gives, for a fixed porosity, the value of hydrostatic stress that will produce dilatational plastic deformation. The present viscoplastic formulation cannot be used in the purely hydrostatic limit without encountering mathematical singularities. Such a case, however, can still be treated approximately in the limit of high triaxialities, when the hydrostatic component is much larger than the deviatoric one. In what follows, we will fit the parameter $\alpha(X, \phi)$ by matching the result of the self-consistent formulation to the Gurson equation (40) for aggregates with the lowest possible anisotropy and rate-sensitivity. For this fitting procedure the VPSC model has been applied to an fcc aggregate, with 500 randomly oriented spherical grains deforming by $(1\,1\,1)\langle 1\,1\,0\rangle$ slip, containing spherical voids, and using a rate-sensitivity exponent $n = 20$ (considered in what follows as the "rate-insensitive limit"). The loading conditions chosen for the fitting correspond to an axisymmetric tensile stress. We are aware that the resulting values of $\alpha(X, \phi)$ are influenced by a number of assumptions made along the fitting procedure, namely: (a) the exponent ($n = 20$) considered as "rate-insensitive limit"; (b) the characteristics of the texture (number of random grains, crystal type) assumed to represent an isotropic medium; (c) the particular stress state (i.e., axisymmetric) used to impose different triaxialities. In the latter case, a different stress state having associated the same triaxiality (i.e. same first and second invariants) but having a different third invariant, could lead to different α-values. In any case, the forthcoming applications of the extended VPSC formulation correspond to axisymmetric stress states, consistent with the adopted fitting procedure of $\alpha(X, \phi)$.

In the case of a rate-dependent material, a "yield stress" cannot be defined un-ambiguously because any non-zero stress state will induce a strain-rate. Therefore, if the yield surface of a rate-independent material (such as Gurson's yield surface) is assumed to follow from a plastic potential, it should be compared to a surface of equal dissipation-rate of the rate-dependent material. Evidently, the locus of an equal-dissipation-rate surface will depend on the reference dissipation-rate chosen. Lebensohn et al. (2003) show that the dissipation-rate obtained with VPSC is a ho-mogeneous function of degree $(n + 1)$ of the stress. As a consequence, all the equal-dissipation-rate surfaces are homothetic and a unique surface is obtained after normalization. In this work we use the equivalent stress Σ^d induced by a tensile im-posed strain-rate of unit norm in a material without voids, as our normalization stress. The locus of the equal-dissipation-rate defined by the normalized deviatoric stress, the normalized hydrostatic stress, and the porosity, can be directly compared with the rate-independent Gurson yield surface. By adjusting the value of α for parametric val-ues of porosity and triaxiality, the stress predicted by VPSC is made to reproduce the stress state given by the Gurson criterion (Eq. (40)).

Fig. 1a (solid lines) shows 2D sections of the normalized Gurson yield surfaces for different porosities, together with several points of the normalized equal-dissipation-rate surfaces, obtained with VPSC for different positive triaxialities, using the value of α that optimizes the matching with the Gurson surface. The higher the void concentration and/or the imposed hydrostatic state (i.e., the higher local fluctuations inside a grain), the higher the value of α (i.e., the softer effective behavior of the grain). Fig. 1b shows parametric curves of α vs. porosity, for fixed triaxiality, and vice-versa. For the sake of completeness, although the above fitting was done for tensile states, using symmetry arguments it is easy to prove that, for compressive states ($\Sigma^s < 0 \Rightarrow X < 0$), it holds that $\alpha(X, \phi) = \alpha(|X|, \phi)$. Concerning the computational implementation of the model, the above information has been used to build an interpolation table, which gives α for the current porosity and triaxiality.

The adjustment of α above, is done matching the VPSC stress to the Gurson stress, under the condition of equal-dissipation-rate. No constraint is imposed on the associated strain-rate. Within the Gurson criterion, the latter follows from the associated flow rule (also called normality rule). Within the viscoplastic polycrystal approach, however, the strain-rate follows from the calculation, and is not assumed to be given by the nor-mality rule. Our calculation shows that in our model the coincidence of the plastic potential and the yield surface is only approximate, and becomes more non-associative with increasing porosity and triaxiality. Fig. 2 (left column) shows polar charts display-ing the relative deviation between VPSC's and Gurson's strain-triaxiality at different stress-triaxialities, for two different porosities. This difference in the strain-triaxiality predicted by both models can be interpreted into angular deviations of VPSC strain-rates from the normal to the yield surface, and is shown in the plots on the right of Fig. 2. At 0.1% porosity we see that, moving from low to high stress-triaxialities, VPSC overes-timates Gurson's strain-triaxialities. This disagreement determines deviations of VPSC from the normality condition, which starts becoming noticeable for triaxialities higher than 3. At a higher porosity (1%), VPSC overestimates Gurson's strain-triaxialities by about 25–50%, for the whole range of triaxialities considered. This determines a
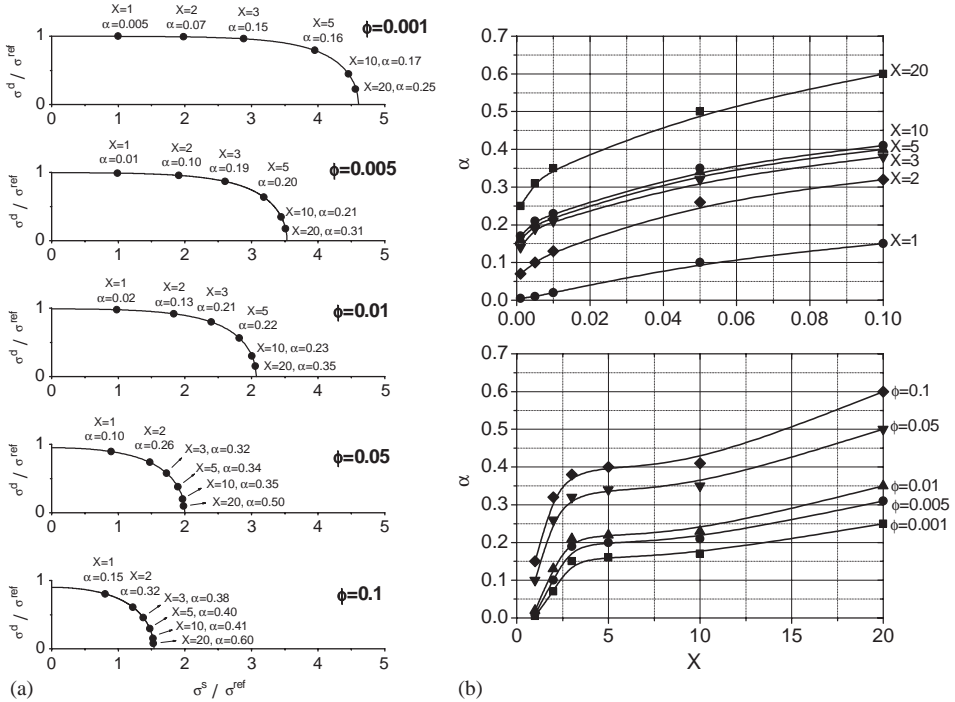
Fig. 1. (a) Normalized Gurson yield surface (solid lines) for porosities 0.1%, 0.5%, 1%, 5% and 10% and points of the normalized equal-dissipation-rate surface, for same porosities and triaxialities 0, 1, 2, 3, 5, 10 and 20, calculated with VPSC for the displayed value of the super-tangent parameter α, for the case of a fcc polycrystal with random crystallographic texture, spherical grains, spherical voids and viscoplastic exponent $n = 20$. (b) Dependence of α as a function of porosity for parametric triaxialities and vice versa.

deviation from normality which is close to $20°$ when $X = 5$ and is even higher for higher triaxialities.

2.7. Algorithm

To illustrate the use of this formulation, we describe here the steps required to predict the rate of porosity evolution $\dot{\phi}$ for a given stress state Σ_{ij}, applied to a polycrystal with an initial porosity ϕ. From Σ_{ij} we can derive the mean stress Σ^s, the stress deviator Σ_{ij}^d, the equivalent deviatoric stress Σ^d and the triaxiality X. With ϕ and X, the value of the super-tangent parameter $\alpha(X, \phi)$ can be obtained. In order to start an iterative search of the local states, one should assume initial input values for the local deviatoric stresses and moduli. Taking $\sigma_{ij}^d = \Sigma_{ij}^d$, initial guesses for $\dot{\varepsilon}_{ij}^d, M_{ijkl}$ and $\dot{\varepsilon}_{ij}^{do}$ can readily be obtained for each grain. Next, we use simple averages of the corresponding local moduli as initial guesses for the macroscopic moduli $\bar{M}_{ijkl}, \dot{\bar{E}}_{ij}^{do}$ and $\bar{K}$. With them and the applied state Σ_{ij} the corresponding guess for the macroscopic strain-rate follows from the constitutive law (Eq. (3)), and the Eshelby
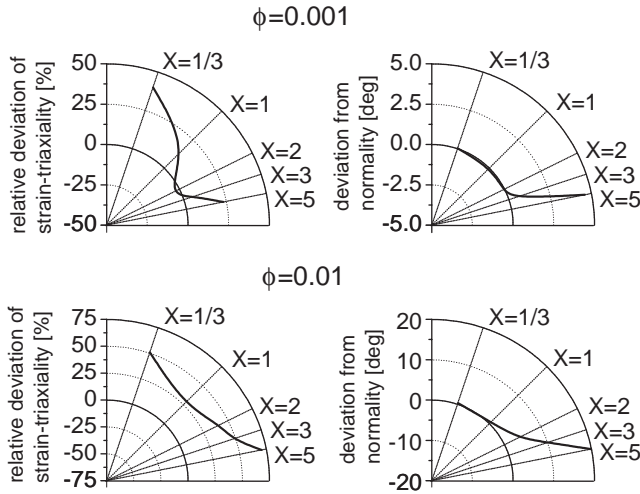
Fig. 2. Deviation of VPSC from Gurson as a function of stress triaxiality, for porosities 0.1% and 1%, left: relative strain-triaxiality deviations, right: angular deviation from normality.

tensors and factors S_{ijmn}^{d}, S_{ij}^{s}, Ψ and β_{ij}^{s} can be calculated using the macroscopic moduli and the grain and void shapes. Subsequently, the interaction tensors and factors $\tilde{M}_{ijkl}$, $\tilde{\beta}_{ij}$ and $\tilde{K}$ (Eqs. (25)), and the localization tensors B_{ijkl}, Φ_{ij}, B^{s}, A_{ijkl}, Ω_{ij} and A^{s} (Eqs. (27), (30) and (31)) can be obtained as well. With these tensors, new estimates of $\bar{M}_{ijkl}$, $\dot{E}_{ij}^{do}$ and $\bar{K}$ are obtained by means of the selfconsistent equations (37). After achieving convergence on the macroscopic moduli (and, consequently, also on the macroscopic strain-rate and the interaction tensors and factors), new estimates of the local stresses can be obtained using the interaction equations (24). If the recalculated local stresses are different from the input values, a new iteration is started. If, instead, they coincide within a certain tolerance, the converged value of the macroscopic bulk modulus $\bar{K}$ is used to obtain the macroscopic dilatation-rate as: $\dot{E}^{s} = \Sigma^{s}/\bar{K}$. Finally, the porosity-rate is calculated by means of the following kinematic relation (Tvergaard, 1981):

$$\dot{\phi} = (1 - \phi)\dot{E}^{s}. \tag{43}$$

3. Results

In this section we present several calculations that illustrate the capabilities of the extended VPSC formulation, and compare its predictions with the ones obtained using the classical Gurson model. We show in what follows how this formulation accounts not only for porosity evolution, but also for void shape effects in the mechanical response and in the porosity evolution. The effect of rate-sensitivity, texture and
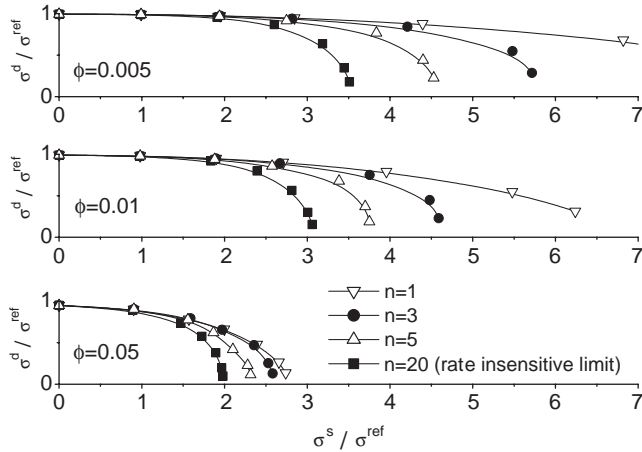
Fig. 3. Effect of rate-sensitivity. Normalized equal-dissipation-rate surfaces, for porosities 0.5%, 1% and 5%, calculated with VPSC for a random fcc polycrystal with spherical voids, for different rate-sensitivity exponents.

triaxiality upon the mechanical response of a voided material is also investigated in this section.

3.1. Effect of rate-sensitivity

One interesting characteristic of the present formulation is that its results depend on the rate-sensitivity of the material. This feature can be easily visualized by plotting normalized equal-dissipation-rate surfaces, corresponding to different rate-sensitivity exponents. Fig. 3 shows these surfaces for 0.5%, 1% and 5% porosity, calculated with VPSC for a random polycrystal with spherical voids, using rate-sensitivity exponents $n = 1, 3, 5$ and 20 (the latter is regarded here as the rate-insensitive limit). Even though the associated flow rule does not apply, it is still true that the normal to the equal-dissipation-rate surface gives a qualitative estimate of the strain-rate triaxiality (see discussion above). An inspection of the sections in Fig. 3 indicates that:

(a) At a given porosity and for fixed stress triaxiality (straight line through the origin), the higher the rate-sensitivity (lower exponent) the smaller the dilatation component $\dot{E}^s$ and, as a consequence, the lower the required strain triaxiality (defined as $\dot{E}^s/\dot{E}^d$). In other words, the porosity evolution (dilatation-rate) will be slower for the same stress triaxiality because the solid phase contributes more to overall deformation as the rate-sensitivity of the material increases.

(b) As the porosity increases, the relative difference between the surfaces corresponding to different rate-sensitivities decreases. In other words, the material becomes less rate-sensitive as porosity increases, since the cavities themselves are, essentially, rate-insensitive domains. The same tendency was reported by Liu et al. (2000) using a rate-sensitivity extension of the Gurson model.
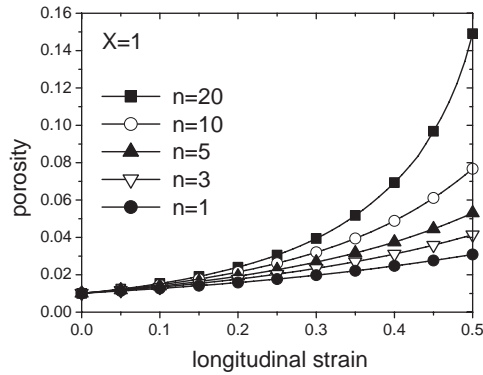
Fig. 4. Effect of rate-sensitivity on porosity evolution, for a random polycrystal with spherical voids, deforming in tension, for $X = 1$ and different rate-sensitivity exponents. Initial porosity: 1%. Total longitudinal strain: 0.5.

In Fig. 3 we show equal-dissipation-rate sections, corresponding to fixed porosities and different triaxialities. An alternative representation is to show the porosity evolution associated with a fixed triaxiality. In Fig. 4 we plot the porosity evolution of a random fcc polycrystal with 1% initial volume fraction of spherical voids, for different values of the rate-sensitivity exponent and a fixed triaxiality $X = 1$. Evidently, the present model predicts a faster porosity evolution as the rate-sensitivity of the solid material decreases.

3.2. Effect of void morphology

In order to isolate the effects of void morphology from the full anisotropy evolution due to morphologic and crystallographic texture development, we ran simulations where neither texture development nor void morphology evolution were allowed. Fig. 5 shows the VPSC predictions of porosity evolution during a triaxial creep test, for a random fcc polycrystal with different void shapes (spherical, oblate and prolate) and for triaxialities $X = 1/3$ (uniaxial stress) and $X = 1$. In the oblate (prolate) case, the short (long) axis of the ellipsoidal void is aligned with the tensile axis. In all cases the rate-sensitivity exponent is $n = 10$, initial porosity is 0.5%, and the total longitudinal strain imposed is 0.5. Note that scales are different since, as expected, porosity increases faster at the higher triaxiality. Oblate voids (axes ratios 5:5:1) tend to grow significantly faster than prolate ones (axes ratios 1:1:5), independent of the triaxiality. This intuitively correct result has also been reported by other authors, using different approaches (Lee and Mear, 1991; Ponte Castañeda and Zaidman, 1996). Under the present model, the void morphology enters naturally into the formulation via the Eshelby tensor, whose components depend on the orientation and the shape of the cavities present in the material (see Section 2.3). In addition, it is possible to treat both aligned or arbitrarily distributed void shapes. In the former case, the Eshelby tensor is the same for all the voids, while the latter case requires
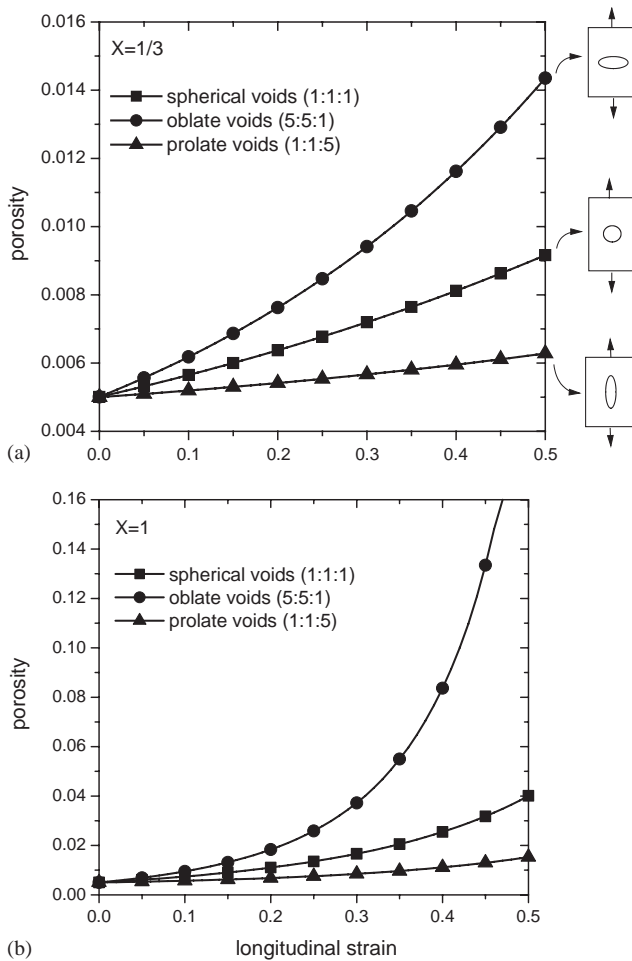
Fig. 5. Effect of void shape. VPSC predictions of porosity evolution during a creep test performed on an fcc polycrystal with random texture, for different void morphologies, with no texture or morphology evolution. Initial porosity: 0.5%, $n = 10$, total longitudinal strain: 0.5. Cases of: (a) triaxiality 1/3, (b) triaxiality 1.

calculating the Eshelby tensor for each void, which results in a more time-consuming calculation.

At this point, it is interesting to compare the results of the present theory with those of a Finite Element calculation of a porous viscoplastic unit cell. Fig. 6 shows relative porosity (ϕ/ϕ_o), void aspect-ratio and longitudinal strain, as functions of time, during a creep test, as predicted with VPSC and the corresponding FE results, reported by Garajeu et al. (2000). In both simulations, the initial porosity ϕ_o is 0.1%, the void shape is initially spherical and the rate-sensitivity exponent is $n = 5$. Cases for two different triaxialities ($X = 0.762$ and 1.833) are compared. At a lower triaxiality, VPSC slightly overestimates porosity evolution while, at a higher triaxiality, porosity evolution
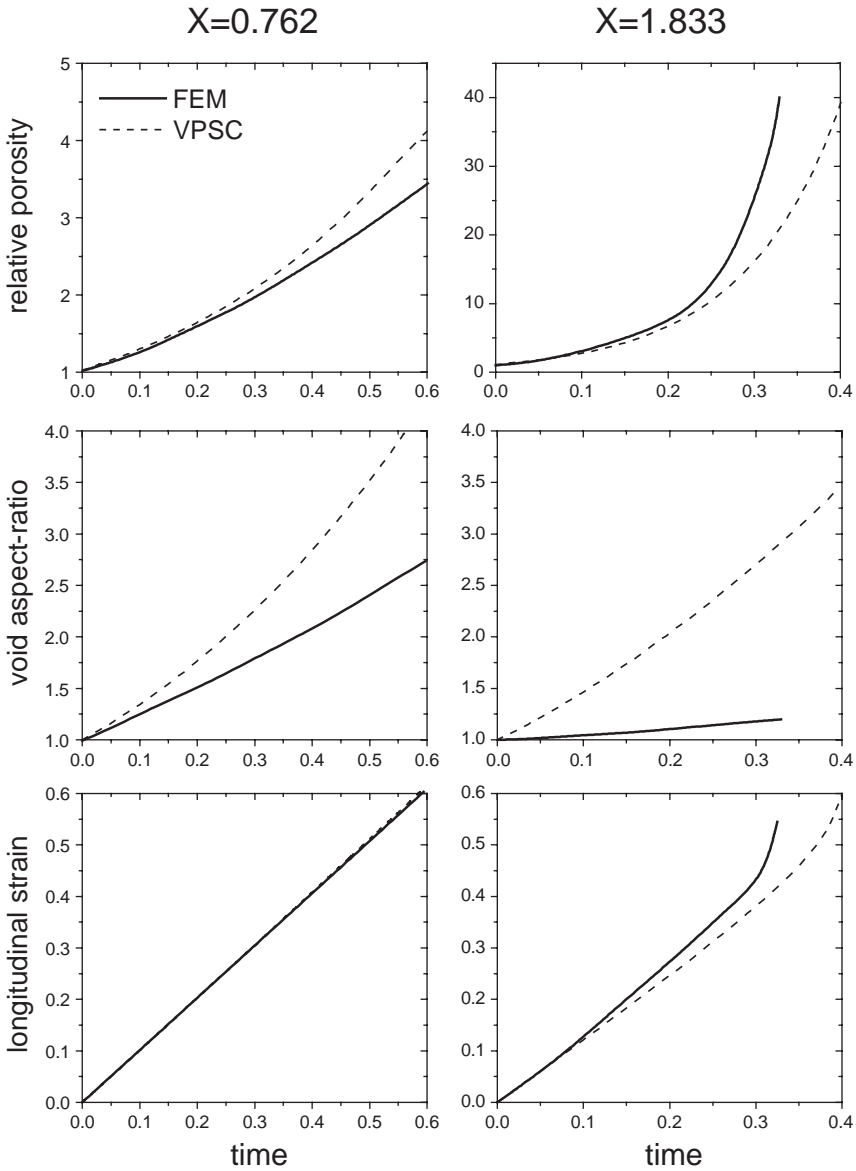
Fig. 6. Comparison with FEM results. Finite Element predictions for a 3D porous viscoplastic unit cell (after Garajeu et al., 2000) vs. VPSC predictions of: relative porosity (ϕ/ϕ_o), void aspect-ratio and longitudinal strain as function of time. Initial porosity: $\phi_o = 0.1\%$; initial void shape: spherical; rate-sensitivity: $n = 5$. Cases for two different triaxialities: $X = 0.762$ and 1.833.

and, consequently, longitudinal strain are underestimated by VPSC. Moreover, for both triaxilities considered here, VPSC overestimates the void aspect-ratio evolution, with respect to FE results. The underestimation of porosity evolution (and, consequently,

of longitudinal strain) at high triaxialities (i.e., when the volume fraction of voids undergoes a rapid increase) can be ascribed to the lack of void interaction, implicit in the VPSC formulation. As a matter of fact, Garajeu et al. (2000) showed, using their micromechanical approach, that the consideration of void interaction ("distribution effects" in their terminology) speeds up the predicted porosity evolution, compared with similar calculation, without consideration of those effects.

3.3. Coupling between texture development and porosity evolution

The present model allows us to account for the anisotropic response of voided polycrystals induced by the development of crystallographic and/or morphologic texture. While the former is due to crystal rotations associated with plastic distortion of the grains, the latter refers to changes in the shape of both, voids and grains. Fig. 7a shows the porosity evolution in an fcc polycrystal, with initially random crystallographic texture, a rate-sensitivity exponent $n = 10$, an initial porosity of 1%, for a simulation of an axisymmetric creep test with a triaxiality $X = 1$ and total longitudinal strain of 0.5. The different cases are for voids of different initial shapes (spherical or prolate with a long/short ratio of 5), with or without texture evolution. When no crystallographic texture development is allowed, in all the cases the final porosities remain below 10%. As discussed in Section 3.2, prolate voids tend to grow slower than spherical voids. Moreover, if the initially spherical voids are allowed to evolve in shape under such a stress state, they become prolate and the porosity exhibits a slightly slower evolution. On the other hand, if the crystallographic texture is allowed to evolve, the tensile axis tends to align with the $\langle 1\,1\,1 \rangle$ crystallographic direction (a secondary component develops along the $\langle 1\,0\,0 \rangle$ direction), the solid phase (grains) become harder to deform along this direction, and as a consequence more deformation is accommodated by the void phase (compare open and solid symbol curves). In the cases of fixed void shape, once again prolate voids grow slower than spherical voids. In the case of evolving shape, although the voids go from spherical to prolate shape, the porosity grows even faster than in the former cases, indicating a strong coupling between texture, morphologic effects and porosity evolution.

In what concerns the effect of porosity on texture, in the right side of Fig. 7a we report the final intensities of the $\langle 1\,1\,1 \rangle$-peak of the inverse pole figure, corresponding to the three cases with texture evolution. It can be seen that, if the porosity evolves faster (slower), the deformation carried out by the solid material is smaller (higher) leading to a slower (faster) crystallographic texture evolution. Finally, Fig. 7b shows that the evolving morphology of the cavities is also affected by the anisotropy evolution of the voided polycrystal. Comparing the void aspect-ratio predicted with and without crystallographic texture evolution, it is seen that in the former case the voids become more elongated than in the latter one, for the same amount of macroscopic elongation.

The previous example shows that the anisotropy induced by texture development in a polycrystal with initial random texture gradually affects the porosity evolution. As a consequence, it is to be expected that a simulation carried out in an initially textured polycrystal along different directions should predict a different trend of void
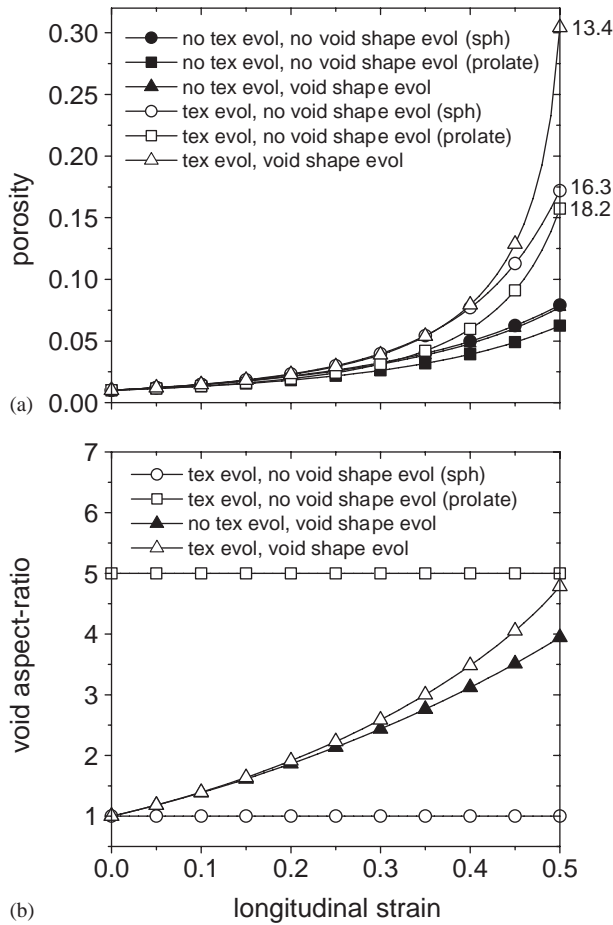
Fig. 7. Effect of texture development. Evolution of (a) porosity and (b) void aspect ratio during a creep test performed on an fcc polycrystal with random texture, for different void morphologies, with and without texture and/or morphology evolution. Initial porosity: 1%, $X = 1$, $n = 10$, total longitudinal strain: 0.5. In the cases with texture evolution, the final (1 1 1) inverse pole figure intensity is indicated (numbers at the left).

growth, from the very beginning of the deformation. Furthermore, this anisotropic be-havior should be more marked if the plastic anisotropy of the single crystal is higher. For this reason, the next example concerns texture and porosity evolution simula-tions carried on an hcp material, with easy $(0\,0\,0\,1)\langle1\,\bar{2}\,1\,0\rangle$ basal and $(1\,0\,\bar{1}\,0)\langle1\,\bar{2}\,1\,0\rangle$ prismatic $\langle a \rangle$ slip and four times harder $(1\,0\,\bar{1}\,1)\langle1\,1\,\bar{2}\,3\rangle$ pyramidal $\langle c + a \rangle$ slip and an initial texture consisting of a strong basal component along the axis x_1 (Fig. 8c, left). The imposed stress states were axisymmetric, with the tensile axis parallel to x_1 or parallel to x_2, with a constant axial strain-rate of $1\,\mathrm{s}^{-1}$ and constant lateral stresses chosen to give an initial triaxiality of 1. The initial porosity was 1% of spherical voids and the final longitudinal strain was 0.5. Other conditions of these
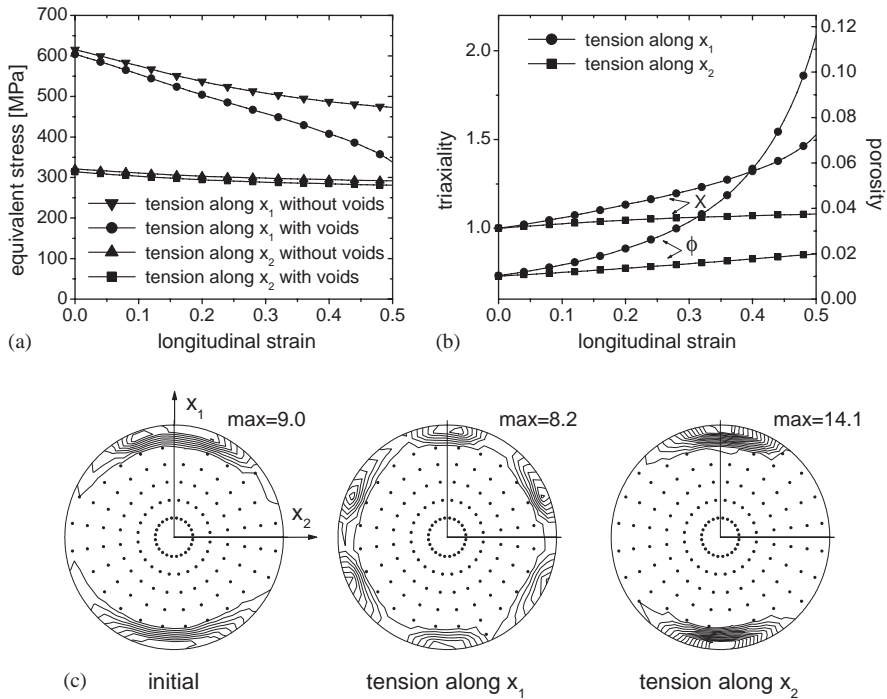
Fig. 8. Coupling between initial texture and porosity evolution. VPSC predictions of (a) stress–strain curves for a textured hcp polycrystal, deformed in tension along x_1 and x_2, at a constant longitudinal strain-rate of 1 s^{-1} and an initial triaxiality of 1. Cases with and without porosity. (b) corresponding porosity (right axis) and triaxiality (left axis) evolution. (c) initial and final (0 0 0 1) basal poles figures. Initial porosity: 1%, $n = 10$, prismatic and basal slip ($\tau^s = 100$ MPa) and pyramidal $\langle c + a \rangle$ slip ($\tau^s = 400$ MPa). Total longitudinal strain: 0.5.

simulations were: $n = 10$, texture and morphology evolution allowed, and no mechanical strain-hardening (i.e., constant threshold stresses for every slip system throughout deformation).

Fig. 8 shows (a) the predicted stress–strain curves (including analogous cases without voids), (b) the triaxiality and porosity evolution and (c) the initial and final textures. It can be seen that the texture evolution depends on the orientation of the tensile axis relative to the initial texture (Fig. 8c) and, that the porosity evolution is also strongly influenced by the direction of loading, relative to the texture (Fig. 8b). Indeed, the case of tension along x_1 (i.e. most crystals with their $\langle c \rangle$-axis aligned in tensile direction and therefore hard to deform) exhibits a faster void growth than the case of tension along x_2. The reason for this is that the material chooses to accommodate deformation by opening the voids, rather than by deforming plastically along the hard direction. The coupling between the hydrostatic component and the material plastic anisotropy is strong: the hydrostatic component leverages the latter mechanism, and promotes the void contribution to deformation. The response of this hcp aggregate

provides a dramatic example of a case where the combined anisotropy of the single crystal and of the polycrystal (texture) affect the evolution of porosity substantially. The difference in porosity evolution predicted above when the textured hcp plate is made to deform in tension along different directions, should also manifest itself in the overall mechanical response. Note that, unlike a creep test simulation, these mixed boundary conditions determine changes in triaxiality (an increase, in these cases) as deformation proceeds (Fig. 8b). The stress–strain curves (Fig. 8a) without porosity show a geometric softening consistent with the texture evolution shown in Fig. 8c. Furthermore, if the textured plate is initially voided and porosity evolution is allowed, in the case of tension along x_1 a fast porosity evolution induces a significant additional softening (and, consequently, a marked increase of the triaxiality), while, in the case of tension along x_2, the contribution to softening of the slow porosity evolution is only marginal.

4. Conclusions

We have presented here an extension of the polycrystal VPSC model which incorporates a viscoplastic compressibility to the originally incompressible approach. The motivation for this extension is to be able to account for porosity and its evolution during plastic forming, while retaining the capabilities of the VPSC formulation. Specifically, we are interested in retaining the crystallographic basis of the model, and its description of anisotropy and anisotropy evolution both at the grain and at the aggregate level. We also retain the rate-sensitivity effects built in the model. The benefits of extending the VPSC formulation, however, go beyond the specific problem of damage evolution. By forcing us to reformulate the model in terms of a more general linearization of the material response (which supercedes the traditional secant or tangent assumptions), we can now account (albeit approximately) for variations of stress and strain-rate in the grains. Such a super-tangent extension is based on the affine formulation for viscoplasticity, proposed by Masson et al. (2000).

It is unavoidable, when referring to plasticity models which include porosity, to compare them with the widely used seminal model proposed by Gurson (1977). The present VPSC extension has advantages and disadvantages when compared to the Gurson model. Among the advantages: (1) VPSC accounts for the anisotropy of the mechanical response, while Gurson is limited to an isotropic response; (2) VPSC accounts for ellipsoidal void shapes and shape evolution with deformation, while Gurson assumes spherical voids; (3) rate-sensitivity effects are not accounted for by the Gurson formulation. Among the disadvantages: (1) VPSC is based on a linearization of a highly non-linear rate-sensitive constitutive response and, as a consequence, it becomes less accurate when spatial inhomogeneity is large. This handicap is partially mitigated with the introduction of the super-tangent approach; (2) VPSC cannot handle purely hydrostatic stress states, although from an algorithmic point of view one can handle stress triaxialities up to $X = 20$; (3) from a numerical point of view, VPSC is much more complex to implement than Gurson, and much more demanding on computer resources. In addition, VPSC gives a non-associative response, which in some cases could be use-

ful for dealing with materials that might exhibit such non-associative behavior, under specific conditions.

Obviously, the reason for choosing VPSC over Gurson (or over one of the various Gurson extensions proposed in the literature) depends on the characteristics of the material and the loading conditions under consideration. When anisotropy and its evolution with deformation have to be accounted for, or when void shape matters, then we show in this work that VPSC does a good job at simulating the mechanical response and porosity evolution. We may say that, in much the same way as the original VPSC formulation represents an improvement over the limited isotropic Von Mises plastic approach, the present extension represents an improvement over the simple isotropic Gurson formulation.

The present extended VPSC model contains one tunable parameter $\alpha(\phi, X)$, a function of the porosity and the triaxiality, which controls the linearization of the constitutive response. This parameter is tuned to give the same response as Gurson when the material has low rate-sensitivity, is isotropic and the cavities are spherical. A direct connection exists between this parameter and the second order stress moments associated with the stress gradients in the grains, required to accommodate locally the deformation of the voids. Such second order moment dependence was formally introduced by Ponte Castañeda (1991, 2002a, b) in his variational formalisms.

We explore here the predictions of the extended VPSC formulation for a variety of situations. Specifically we test the effect of void shape, texture, strain-rate, and triaxiality upon damage evolution, texture evolution and stress–strain response. In all these cases the results obtained are qualitatively in agreement with the intuitive response that one expects and also with those of other micromechanical approaches and FE calculations. For example, we predict that:

(a) Superimposing a hydrostatic stress component increases the rate of void dilatation and, consequently, their contribution to deformation.
(b) Void shape has a major effect on porosity evolution. Oblate voids tend to grow faster than prolate voids under tensile stress, and lead to accelerated damage evolution.
(c) Rate-sensitivity influences porosity evolution in such a way that, under tensile stress, voids tends to grow faster in less rate-sensitive materials.
(d) Texture can change substantially the porosity evolution in a highly anisotropic hexagonal aggregate tested along and across the main texture component. The reason is that it is more efficient for the material to accommodate deformation by deforming the voids rather than the hard grains.

This extended VPSC model will have to be tested and expanded in the future. Experimental verification should be an important part of such effort, and processing materials having well-controlled initial porosity and texture, and performing well-controlled experiments, will certainly be a challenge. From a numerical perspective, we plan to use the model to describe the local constitutive response in FEM simulations of plastic forming operations. Criteria for void nucleation can be incorporated straightforwardly into the formulation, as well as distributions of void shapes. It will be

more challenging to incorporate void coalescence effects, and a dependence of the model with the relative size of voids and grains (size effects). Finally, we plan to study the model performance when simulating aggregates of material grains (no voids) with very inhomogeneous properties. The possibility of accounting for intragranular gradients and localization through second order moments should open new avenues in this area, and should provide a more efficient tool for modeling these systems.

Acknowledgements

Appendix. Green function method and Fourier transform solution

System (7) consists of four differential equations with four unknowns: three are the components of velocity deviation vector $\tilde{u}_i(\bar{x})$, and one is the mean stress deviation $\tilde{\sigma}^s(\bar{x})$. Applying the Green function method and Fourier transforms the solution of differential system (7) can be found by solving the following algebraic system (Lebensohn et al., 2003):

$$\alpha_j \alpha_l \bar{L}_{ijkl} k^2 \hat{G}_{km}(\bar{k}) + \alpha_i ik \hat{H}_m(\bar{k}) = \delta_{im}, \tag{A.1a}$$

$$\alpha_k k^2 \hat{G}_{km}(\bar{k}) - \bar{K}^{-1} ik \hat{H}_m(\bar{k}) = -\bar{K}^{-1} ik \delta_{4m}, \tag{A.1b}$$

where $\hat{G}_{km}$ and $\hat{H}_m$ are the Fourier transforms of the Green functions associated with the velocity and the mean stress fields, respectively, and k and $\bar{\alpha}$ are the modulus and the unit vector associated with a point of Fourier space $\bar{k}$ (i.e., $\bar{k} = k\bar{\alpha}$), respectively. Calling $A_{ik}^d = \alpha_j \alpha_l \bar{L}_{ijkl}$, system (A.1) can be expressed as a matrix product $A \times B = C$ where A, B and C are 4×4 matrices given by

$$
A = \begin{vmatrix} A_{11}^d & A_{12}^d & A_{13}^d & \alpha_1 \\ A_{21}^d & A_{22}^d & A_{23}^d & \alpha_2 \\ A_{31}^d & A_{32}^d & A_{33}^d & \alpha_3 \\ \alpha_1 & \alpha_2 & \alpha_3 & -\bar{K}^{-1} \end{vmatrix}
\begin{vmatrix} k^2 \hat{G}_{11} & k^2 \hat{G}_{12} & k^2 \hat{G}_{13} & k^2 \hat{G}_{14} \\ k^2 \hat{G}_{21} & k^2 \hat{G}_{22} & k^2 \hat{G}_{23} & k^2 \hat{G}_{24} \\ k^2 \hat{G}_{31} & k^2 \hat{G}_{32} & k^2 \hat{G}_{33} & k^2 \hat{G}_{34} \\ ik\hat{H}_1 & ik\hat{H}_2 & ik\hat{H}_3 & ik\hat{H}_4 \end{vmatrix} = B
$$

$$
\begin{vmatrix} 1 & 0 & 0 & 0 \\ 0 & 1 & 0 & 0 \\ 0 & 0 & 1 & 0 \\ 0 & 0 & 0 & -ik\bar{K}^{-1} \end{vmatrix} = C. \tag{A.2}
$$

The matrix A is real and symmetric. As a consequence, its inverse will also be real and symmetric. Using the explicit form of matrix C, we can write the solution to (A.1) as

$$
B = A^{-1} \times C = \begin{bmatrix}
A_{11}^{-1} & A_{12}^{-1} & A_{13}^{-1} & -(ik\bar{K}^{-1})A_{14}^{-1} \\
A_{21}^{-1} & A_{22}^{-1} & A_{23}^{-1} & -(ik\bar{K}^{-1})A_{24}^{-1} \\
A_{31}^{-1} & A_{32}^{-1} & A_{33}^{-1} & -(ik\bar{K}^{-1})A_{34}^{-1} \\
A_{41}^{-1} & A_{42}^{-1} & A_{43}^{-1} & -(ik\bar{K}^{-1})A_{44}^{-1}
\end{bmatrix}. \tag{A.3}
$$

Finally, comparing (A.2) and (A.3),

$$
k^2 \hat{G}_{ij} = A_{ij}^{-1} \quad (i,j = 1,3), \tag{A.4}
$$

$$
k^2 \hat{G}_{i4} = -(ik\bar{K}^{-1})A_{i4}^{-1} \quad \Rightarrow \quad (ik\bar{K})\hat{G}_{i4} = A_{i4}^{-1} \quad (i = 1,3). \tag{A.5}
$$

Since the components of A are real functions of α_i, so are the components of A^{-1}, and so $k^2 \hat{G}_{ij}$ and $ik\hat{H}_i$ are real functions of α_i. This property leads to real integrals in the derivation that follows.

The velocity field can be written in terms of convolution integrals between the corresponding Green tensors and the inhomogeneity fields. The local deviation in velocity is given by

$$
\tilde{u}_k(\bar{x}) = \int_{R^3} G_{ki}(\bar{x} - \bar{x}') f_i^{\mathrm{d}}(\bar{x}') \, \mathrm{d}\bar{x}' + \int_{R^3} G_{k4}(\bar{x} - \bar{x}') f^{\mathrm{s}}(\bar{x}') \, \mathrm{d}\bar{x}'. \tag{A.6}
$$

Taking partial derivatives to (A.6), replacing the explicit expressions of f_i^{d} and f^{s} (Eqs. (8) and (9)), recalling that $\partial G_{ij}(\bar{x} - \bar{x}')/\partial\bar{x} = -\partial G_{ij}(\bar{x} - \bar{x}')/\partial\bar{x}'$, integrating by parts, and using the divergence theorem, we obtain

$$
\tilde{u}_{k,l}(\bar{x}) = -\int_{R^3} G_{ki,jl}(\bar{x} - \bar{x}')\bar{L}_{ijmn}\dot{\varepsilon}_{mn}^{\mathrm{d}*}(\bar{x}') \, \mathrm{d}\bar{x}' - \int_{R^3} G_{k4,l}(\bar{x} - \bar{x}')\bar{K}\dot{\varepsilon}^{\mathrm{s}*}(\bar{x}') \, \mathrm{d}\bar{x}'. \tag{A.7}
$$

Eq. (A.7) provides an exact implicit solution to the problem. Such solution requires knowledge of the local dependence of the eigen-stress tensor. However, we know from the elastic Eshelby's inclusion formalism that if the eigen-strain is uniform over an ellipsoidal domain where the stiffness tensor is uniform, then the stress and the strain are constant over the domain of the inclusion. The latter suggests to assume a constant eigen-strain-rate of constant value (a priori unknown) within the volume Ω of the inclusion, and zero outside. This allows us to average the local field (A.7) over the domain Ω and obtain an average strain-rate inside the inclusion. Expressing the Green

tensor in terms of its inverse Fourier transform and taking derivatives we obtain

$$\tilde{u}_{k,l} = \left(\frac{1}{8\pi^3 \Omega} \int_\Omega \int_\Omega \int_{R^3} \alpha_j \alpha_l k^2 \hat{G}_{ki}(\bar{k}) \exp[-i\bar{k}(\bar{x} - \bar{x}')] \, d\bar{k} \, d\bar{x} \, d\bar{x}' \right) \bar{L}_{ijmn} \dot{\varepsilon}_{mn}^{d*}$$

$$+ \left(\frac{1}{8\pi^3 \Omega} \int_\Omega \int_\Omega \int_{R^3} \alpha_l i k \bar{K} \hat{G}_{k4}(\bar{k}) \exp[-i\bar{k}(\bar{x} - \bar{x}')] \, d\bar{k} \, d\bar{x} \, d\bar{x}' \right) \dot{\varepsilon}^{s*}, \quad \text{(A.8)}$$

where $\tilde{u}_{k,l}$, $\dot{\varepsilon}_{mn}^{d*}$ and $\dot{\varepsilon}^{s*}$ have to be interpreted as average quantities inside the grain. The two expressions in parentheses are the Green interaction tensors T_{klij}^d and T_{kl}^s, such that

$$\tilde{u}_{k,l} = T_{klij}^d \bar{L}_{ijmn} \dot{\varepsilon}_{mn}^{d*} + T_{kl}^s \dot{\varepsilon}^{s*}. \tag{A.9}$$

Writing $d\bar{k}$ in spherical coordinates: $d\bar{k} = k^2 \sin\theta \, dk \, d\theta \, d\varphi$, using (A.4) and (A.5), and integrating inside an ellipsoidal grain of radii (a, b, c) (Berveiller et al., 1987) gives

$$T_{klij}^d = \frac{abc}{4\pi} \int_0^{2\pi} \int_0^\pi \frac{\alpha_j \alpha_l A_{ki}^{-1}(\bar{\alpha})}{[\rho(\bar{\alpha})]^3} \sin\theta \, d\theta \, d\varphi, \tag{A.10}$$

$$T_{kl}^s = \frac{abc}{4\pi} \int_0^{2\pi} \int_0^\pi \frac{\alpha_l A_{k4}^{-1}(\bar{\alpha})}{[\rho(\bar{\alpha})]^3} \sin\theta \, d\theta \, d\varphi, \tag{A.11}$$

where $\rho(\bar{\alpha}) = [(a\alpha_1)^2 + (b\alpha_2)^2 + (c\alpha_3)^2]^{1/2}$. The latter expressions have to be integrated numerically (using, for instance, the Gauss–Legendre technique). The evaluation of the integrand requires us to invert a 4×4 matrix (see Eq. (A.2)) for each integration point.

References

Addessio, F.L., Johnson, J.N., 1993. Rate-dependent ductile fracture model. J. Appl. Phys. 74, 1640–1648.

Berveiller, M., Fassi-Fehri, O., Hihi, A., 1987. The problem of two plastic and heterogeneous inclusions in an anisotropic medium. Int. J. Eng. Sci. 25, 691–709.

Carroll, M.M., Holt, A.C., 1972. Static and dynamic pore-collapse relations for ductile porous materials. J. Appl. Phys. 43, 1626–1636.

Chen, B., Xia, Z.C., MacEwen, S.R., Tang, S.C., Huang, Y., 2000. A dilatational plasticity theory for aluminum sheets. In: Chuang, T.J., Rudnicki, J.W. (Eds.), Multiscale Deformation and Fracture in Materials and Structures. Kluwer Academic Publishers, Dordrecht, pp. 17–30.

Chen, B., Huang, Y., Liu, C., Wu, P.D, MacEwen, S.R., 2002. A dilatational plasticity theory for viscoplastic materials. Eng. Fract. Mech., submitted for publication.

Garajeu, M., Michel, J.C., Suquet, P., 2000. A micromechanical approach of damage in viscoplastic materials by evolution in size, shape and distribution of voids. Comput. Methods in Appl. Mech. Eng. 183, 223–246.

Golaganu, M., Leblond, J.B., Devaux, J., 1993. Approximate models for ductile metals containing non-spherical voids-case of axisymmetric prolate ellipsoidal cavities. J. Mech. Phys. Solids 41, 1723–1754.

Golaganu, M., Leblond, J.B., Devaux, J., 1994. Approximate models for ductile metals containing non-spherical voids-case of axisymmetric oblate ellipsoidal cavities. J. Eng. Mater. Tech. 116, 287–290.

Gurson, A.L., 1977. Continuum theory of ductile rupture by void nucleation and growth. J. Eng. Mater. Technol. 99, 2–15.

Hutchinson, J.W., 1976. Bounds and self-consistent estimates for creep of polycrystalline materials. Proc. R. Soc. London A 348, 101–127.

Johnson, J.N., Addessio, F.L., 1988. Tensile plasticity and ductile fracture. J. Appl. Phys. 64, 6699–6712.

Kailasam, M., Ponte Castañeda, P., Willis, J.R., 1997a. The effect of particle size, shape, distribution and their evolution on the constitutive response of nonlinearly viscous composites. I—Theory. Trans. R. Soc. Lond. A 355, 1835–1852.

Kailasam, M., Ponte Castañeda, P., Willis, J.R., 1997b. The effect of particle size, shape, distribution and their evolution on the constitutive response of nonlinearly viscous composites. II—Examples. Trans. R. Soc. Lond. A 355, 1853–1872.

Kailasam, M., Aravas, N., Ponte Castañeda, P., 2000. Porous metals with developing anisotropy: constitutive models, computational issues and applications to deformation processing. Comput. Model. Eng. Sci. 1, 105–118.

Lebensohn, R.A., Canova, G.R., 1997. A selfconsistent approach for modelling texture development of two-phase polycrystals: application to titanium alloys. Acta Mater. 45, 3687–3694.

Lebensohn, R.A., Tomé, C.N., 1993. A selfconsistent approach for the simulation of plastic deformation and texture development of polycrystals: application to zirconium alloys. Acta Metall. Mater. 41, 2611–2624.

Lebensohn, R.A., Solas, D., Canova, G., Brechet, Y., 1996. Modelling damage of Al–Zn–Mg alloys. Acta Mater. 44, 315–325.

Lebensohn, R.A, Turner, P.A., Signorelli, J.W, Canova, G.R, Tomé, C.N., 1998. Calculation of intergranular stresses based on a large strain viscoplastic selfconsistent polycrystal model. Mod. Sim. Mater. Sci. Eng. 6, 447–465.

Lebensohn, R.A., Tomé, C.N., Maudlin, P.J., 2003. An extended self-consistent visco-plastic polycrystal formulation: application to polycrystals with voids. Los Alamos National Laboratory Internal Report LA-UR-03-1193 (electronic version available at: *http://www.lanl.gov/mst/voids.shtml*).

Lee, B.J., Mear, M.E., 1991. Axisymmetric deformation of power-law solids containing a dilute concentration of aligned spheroidal voids. J. Mech. Phys. Solids 39, 45–71.

Liu, C., Huang, Y., Stout, M.G., 2000. On the application of Gurson's theory to voided solids with rate-sensitive matrices, Los Alamos National Laboratory Internal Report LA-UR-2000-1423.

Logé, R., Chastel, Y., Signorelli, J., Lebensohn, R.A., Barberis, P., 1998. Finite element simulation of a zircaloy sheet deep drawing using a polycrystalline model. In: Huétink, J., Baaijens, F.P.T. (Eds.), Simulation of Materials Processing: Theory, Methods and Applications. Balkema, Rotterdam, pp. 329–333.

Masson, R., Bornert, M., Suquet, P., Zaoui, A., 2000. An affine formulation for the prediction of the effective properties of nonlinear composites and polycrystals. J. Mech. Phys. Solids 48, 1203–1227.

Molinari, A., Canova, G.R., Ahzi, S., 1987. A selfconsistent approach of the large deformation polycrystal viscoplasticity. Acta Metall. 35, 2983–2994.

Mura, T., 1988. Micromechanics of Defects in Solids. Martinus-Nijhoff, Dordrecht.

Ponte Castañeda, P., 1991. The effective mechanical properties of nonlinear isotropic composites. J. Mech. Phys. Solids 39, 45–71.

Ponte Castañeda, P., 1996. Exact second-order estimates for the effective mechanical properties of non-linear composite materials. J. Mech. Phys. Solids 44, 827–862.

Ponte Castañeda, P., 2002a. Second-order homogenization estimates for nonlinear composites incorporating field fluctuations. I—Theory J. Mech. Phys. Solids 50, 737–757.

Ponte Castañeda, P., 2002b. Second-order homogenization estimates for nonlinear composites incorporating field fluctuations. I—Applications J. Mech. Phys. Solids 50, 759–782.

Ponte Castañeda, P., Zaidman, M., 1996. Constitutive models for porous materials with evolving microstructure. J. Mech. Phys. Solids 42, 1459–1497.

Suquet, P., 1995. Overall properties of non-linear composites. A modified secant moduli theory and its link with Ponte Castañeda's nonlinear variational procedure. C.R. Acad Sci. Paris IIb 320, 563–571.

Taylor, G.I., 1938. Plastic strain in metals. J. Inst. Met. 62, 307–324.

Tomé, C.N., Maudlin, P.J., Lebensohn, R.A., Kaschner, G.A., 2001. Mechanical response of zirconium. Part I: derivation of a polycrystal constitutive law and finite element analysis. Acta Mater. 49, 3085–3096.

Tvergaard, V., 1981. Influence of voids on shear bands instabilities under plane strain conditions. Int. J. Fract. 17, 389–407.

Tvergaard, V., 1982. On localization in ductile materials containing spherical voids. Int. J. Fract. 18, 237–252.

Walpole, L.J., 1969. On the overall elastic moduli of composite materials. J. Mech. Phys. Solids 17, 235–251.